CrossMark

REVIEW

Determination of Triaxial Residual Stress in Plasma-Sprayed Hydroxyapatite (HAp) Deposited on Titanium Substrate by X-ray Diffraction

N. Bosh[1,2] · H. Mozaffari-Jovein[2] · C. Müller[1]

Abstract Measurement of residual stress in plasma-sprayed coating is of key importance to optimize their microstructure and mechanical properties. In this study, the x-ray diffraction analysis was carried out using the $\sin^2\psi$ method to evaluate the residual stress distribution of hydroxyapatite (HAp) coatings produced on titanium substrate by atmospheric plasma spraying (APS) and vacuum plasma spraying (VPS). The $\sin^2\psi$ method measured strains at different tilt ψ and rotating φ angles around the specimen surface normal. A non-uniform and inhomogeneous stress distribution was present in the both coatings. The measured strain $\varepsilon_{\psi\varphi}$ is plotted versus $\sin^2\psi$, showing a nonlinear (elliptical) behavior, which indicates the presence of inhomogeneous triaxial stress distributions within coating, due to the crystalline anisotropy, inhomogeneous cooling rate or solidification of the molten particles. The normal stress values within both HAp coatings produced were found to be tensile in nature, but the values of tensile stresses are significantly higher in APS coating than those values obtained for VPS coating.

Keywords hydroxyapatite · nanoindentation · plasma spraying · residual stress · titanium · x-ray diffraction

✉ N. Bosh
nasim.bosh@imtek.uni-freiburg.de

[1] Department of Microsystems Engineering, IMTEK, University of Freiburg, Freiburg, Germany

[2] Institut für Werkstoffe und Anwendungstechnik Tuttlingen, IWAT, Hochschule Campus Tuttlingen, Tuttlingen, Germany

Introduction

Hydroxyapatite (HAp) has been widely considered as the most common coating material on the metallic implants to enhance the long-term osseointegration and improve the bioactivity behavior of the metallic surfaces (Ref 1, 2). Because of the similar structural and chemical composition to the bone, HAp can be rapidly integrated into the body issue and improve the bone-to-implant contact (Ref 3). Among the commercial coating deposition techniques, plasma spraying is the most widely used technique for the deposition of HAp due to its high deposition rate, relative ease of operation and low cost (Ref 4). In addition, the major advantage of this process is the ability to deposit coatings onto substrates without significant heat input and varying the microstructure of substrates (Ref 5).

Generally, the durability of thermal spray coating and its adherence to the substrate depend strongly on their microstructure and residual stress present within the coatings (Ref 6, 7). Residual stress often appears in the HAp coatings which were deposited by plasma spraying due to the mismatch of its thermal expansion coefficient (CTE) with the metallic substrate. Thermal stresses can be formed during the spraying process and the following cooling period which can affect the mechanical stabilities, spalling characteristics and fatigue strength of the coated specimens (Ref 8-10). Hence, evaluation of the nature and distribution of internal residual stress (tensile or compressive) produced during deposition is a crucial aspect. Knowledge of the residual stress profiles within coating allows optimizing the spraying techniques, and this effect must be examined more closely.

Measurement of residual stress present in plasma-sprayed HAp coatings has been the subject of some investigations (Ref 11-14). In these investigations, the residual stress is often measured by assuming in-plane

stress state and therefore the stress components and shear stress are often ignored. It should be considered that the homogeneous stress considered so far is an idealization and is only suitable for materials which do not have a complex stress field. Due to the rapid solidification nature of the thermal spray process, the microstructures of the coating produced by this process have essentially anisotropic and non-equilibrium structures including oxide, metastable and amorphous phases (Ref 15). Significant values of residual shear stresses are likely to be created within these coatings due to heterogeneous nature of plasma-sprayed coatings. Nevertheless, studies relating to the inhomogeneous distribution in the residual stress profile have been very limited. For this reason, it is important to identify the full internal stress components within the coating and examine the existence of shear stresses and quantify them to avoid appreciable errors in the calculated values of the principal stresses. Residual stress is one of the most important parameters that affect adhesion of the coating to the substrate, and as such, it is a good practice to analyze them. Coating delamination can be resulted from spallation at the coating/substrate interface due to the high tensile stresses. It is well known that the coatings produced in vacuum have lower stresses that one produced in atmosphere. Therefore, two types of the APS and VPS coatings were selected to analyze to verify the reliability of method used in this study to measure of triaxial HAp coatings.

The aim of this investigation is to evaluate the residual stress distribution as a tensor within the HAp coating deposited on titanium by air plasma spraying (APS) and vacuum plasma spraying (VPS) and to compare their residual stress distributions. In this context, x-ray diffraction was employed as a powerful tool for measurement of the internal stresses of these coatings. The advantage of the x-ray diffraction method is its non-destructive character and the possibility of macro- and micro-stress analysis in multiphase and anisotropic materials. Because of high absorption of x-ray radiation, this method was applied to study residual stresses to the depth of few μm below the surface of sample (Fig. 1). To compensate the potential errors from different grain orientations and increase the accuracy of the calculated stress, a series of scans are performed to locate at least six independent strain measurements by changing the tilt angle ψ (psi) and rotating angle φ (phi) to determine the full mechanical stress tensor of all crystalline phases. The measurement was consequently taken at positive and negative tilt angles ψ to study the shear stresses on the surface. The method can measure components of the stress tensor, i.e., multiaxial stresses, including normal and shear stresses (Ref 16). Determination of the full stress tensor is briefly described and the effects of changing various parameters for producing the HAp coatings and the relationship between microstructure
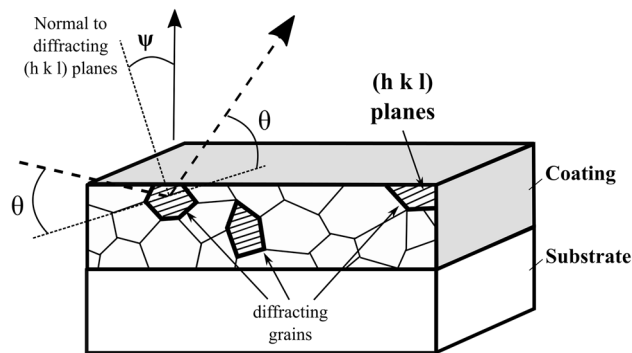

Fig. 1 Schematic of the XRD technique for measurement of residual stresses (ψ is the angle between the lattice plane normal and the sample surface normal)

and residual stresses can be examined, giving insights into possible approaches for controlling residual stress levels and enhancing the mechanical properties and consequently durability of the coating.

Stress Tensor Determination by $\sin^2\psi$ Method

In principle, the $\sin^2\psi$ method can be used to determine full-tensor surface stresses non-destructively in the presence of large subsurface stress gradients. This method is based upon determining changes in crystallographic lattice parameter by measuring of characteristic diffraction peak shifts. The internal stress state in a 3D solid body is represented by three normal stresses and six shear stresses. By considering the state of equilibrium, the stress matrix is symmetric and each pair of shear stresses is equal. This reduces the stress components in the matrix from nine to six independent stresses. The stress tensor in a material can be written as:

$$\sigma = \begin{pmatrix} \sigma_{11} & \tau_{12} & \tau_{13} \\ \tau_{21} & \sigma_{22} & \tau_{23} \\ \tau_{13} & \tau_{23} & \sigma_{33} \end{pmatrix} \tag{Eq 1}$$

where σ_{11}, σ_{22} and σ_{33} are normal stresses; τ_{12}, τ_{13}, τ_{21}, τ_{23}, τ_{13} and τ_{23} are the shear stresses. The residual stress tensor components σ_{ij} of the coating can be calculated by using the elasticity theory via Hooke's law for anisotropic materials and general equation for the triaxial case as:

$$\varepsilon_{ij}^c = s_{ijkl}\sigma_{ij}^c \tag{Eq 2}$$

$$\begin{aligned} \varepsilon_{\varphi\psi}^{hkl} &= \frac{d_{\varphi\psi} - d_0}{d_0} \\ &= \frac{1+v}{E}\left(\sigma_{11}\cos^2\varphi + \tau_{12}\sin 2\varphi + \sigma_{22}\sin^2\varphi - \sigma_{33}\right)\sin^2\psi \\ &\quad + \frac{1+v}{E}\sigma_{33} - \frac{v}{E}(\sigma_{11} + \sigma_{22} + \sigma_{33}) \\ &\quad + \frac{1+v}{E}(\tau_{13}\cos\varphi + \tau_{23}\sin\varphi)\sin 2\psi \end{aligned}$$

$$\tag{Eq 3}$$

where $\varepsilon_{\varphi\psi}^{hkl}$ and $d_{\varphi\psi}$ are strain and inter-planar spacing of h k l in the direction of (φ, ψ), respectively; d_0 is the unstrained inter-planar spacing; υ and E are Poisson's ratio and elastic modulus of the coating. The full mechanical stress tensor composed of normal and shear components of the thin coatings can be determined by $\sin^2\psi$ method with the combination of the tilt angle between the lattice plane normal N and the sample surface normal between the specimen surface normal and the diffraction vector, ψ, with the rotation angle about its surface normal, φ (see Fig. 2). The shifted peaks in the XRD graph are related to the lattice constants changes due to stress in the coating. The complete stress components can be calculated by sets of measurements with positive and negative psi tilts, for three directions (e.g., phi angles 0, 45, 90°). The variation of inter-planar spacing for a reflection in the positive and negative angles ($\pm \psi$ orientation) should be measured to determine if shear stresses are present. The measurement repeated with a sufficient number (6 – 8 Psi tilts for each direction) of measuring points versus $\sin^2\psi$. High ψ ranges minimize the errors in the normal stresses due to stress gradients in the sample.

Obviously, the strain $\varepsilon_{\psi\varphi}$ (measured by peak shift) depends on the angles φ and ψ of the measuring vector. Thus, the shape of the $\varepsilon_{\psi\varphi}$ curve is an indication of the type of stress state that exists within the diffracting volume independent of the type of the material. The components of the mechanical stress tensor can be extracted from slopes of lines, fitted to the lattice-strain data in $\sin^2\psi$-plots and the values of the (h k l)-dependent elastic constants. Generally, four basic types of distribution the measured strains $\varepsilon_{\psi\varphi}$ versus $\sin^2\psi$ can be found, as illustrated in Fig. 3. In the case of linear variation of $\varepsilon_{\psi\varphi}$ versus $\sin^2\psi$, the variation in inter-planar spacing is seen to be the same for both tilt directions ($\pm \psi$ orientations) and no shear components exist in the coating. If shear stresses acting in the planes perpendicular to t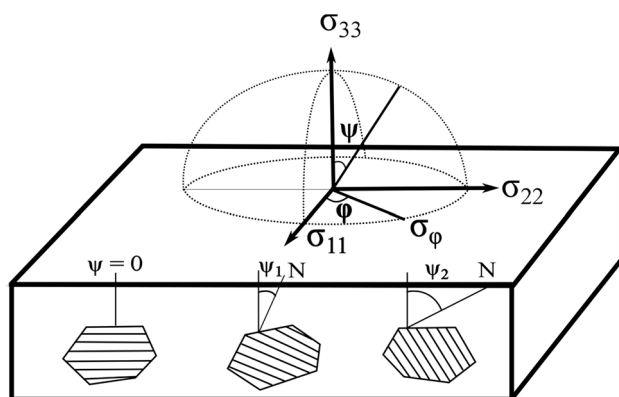he specimen surface are present, they will be manifested by splitting in the $\varepsilon_{\psi\varphi}$ versus $\sin^2\psi$ plot. In this case, the plot is split into two branches of opposite curvature for $\psi > 0$ and $\psi < 0$ and gives an elliptical function (Fig. 3). The $\varepsilon_{\psi\varphi}$ versus $\sin^2\psi$ function can also be much more complicated, and curved plots are attributed to the presence of strong stress gradient along the surface normal of the coating. In the case of crystallographic texture, the $\varepsilon_{\psi\varphi}$ versus $\sin^2\psi$ plot exhibits an elliptical behavior (Ref 16).

Experimental Details

As-received commercial HAp powder material (medipure 20-15/006) with crystal sizes of about 15 to 45 μm was provided by Medicoat Company in France to produce both APS and VPS coatings. This powder is adapted for high bond strength coatings and thermal spray technology and comply with standards ASTM 1185 and 1088; ISO 13779. Commercial pure (cp) titanium grade 4 flat specimens, Φ $5 \times 50 \times 0.5$ mm^3, provided by ARA-T Advance GmbH, Germany, are used as the substrates. Plasma-sprayed HAp coatings must ideally be applied to a grit-blasted roughened surface which provides more surface area for adhesion. Therefore, the surface of the substrates was sandblasted with alumina grit of size 200 μm with compressed air pressure of 5 bar. The specimens were hold in the block heater and preheated prior to deposit of the coating to temperature 400 °C. The substrates were heated while their top surface was spray-coated to improve the coating adhesion and reduce the unfavorable residual stress during cooling. Two groups of coatings were prepared and atmospheric plasma spraying (APS) was performed in ambient air and vacuum plasma spray (VPS), which plasma jet exhausts into a chamber at below atmosphere pressure of 100 mbar. These processes were performed at DLR (Institute of Technical Thermodynamics, Aerospace Center, Stuttgart, Germany). Extensive preliminary work was conducted to optimize the spray parameters and to obtain the same thickness of coatings in both processes. The spray distance was mainly optimized to obtain the adhered coatings with low residual stresses. Low pressure of VPS process produces significant expansion of the isotherms and velocity of the plasma jet, due to the increases in mean free path between the ions and electrons in plasma. Therefore, a spray distance of 80 mm with an injector diameter of 1.8 mm was used for APS coatings, whereas the spray distance is extended to 160 mm with an injector diameter of 3 mm for VPS coatings. Furthermore, for APS coatings, a lower power with only argon gas was used, and for VPS coatings, a higher power was used with helium added to argon. The optimized process parameters are

Fig. 2 Schematic of the stress ellipsoid, which illustrates the basis of the $\sin^2\psi$ technique

Fig. 3 Basic types of possible $\varepsilon_{\psi\varphi}$ vs. $\sin^2\psi$ functions (Ref 16)
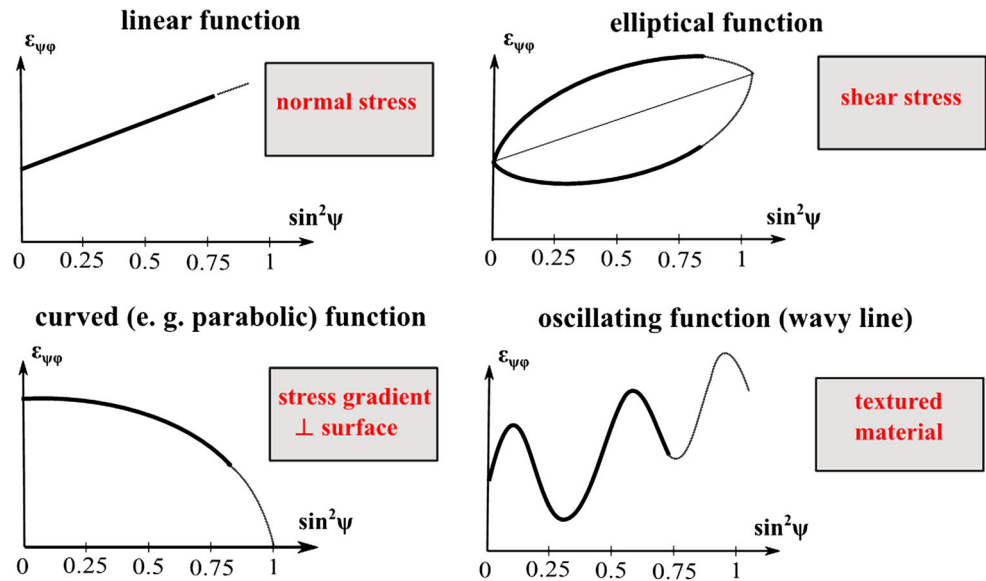
Table 1 Spray parameters to produce HAp coatings used in this study

Process parameters	APS specimen	VPS specimen
Equipment	Triplex Pro210, Oerlikon Metco, Switzerland	F6 Brenner, GTV GmbH, Germany
Plasma gas Ar/He, slpm	40/–	42/20
Spray distance, mm	80	160
Injector diameter, mm	1.8	3
Spraying current, A	500	650
Gun moving speed, mm/s	400	400
Spraying voltage, V	95	48
Electric power, kW	47.5	31

listed in Table 1. A coating of about 50-60 μm was achieved for the both processes.

The elastic behavior of the plasma-sprayed coatings can be different from the elastic behavior of bulk material, owing to their microstructure and reduced dimensionality due to presence of the cracks and porosities in the coating. Hence, the elastic modulus of the HAp coatings, required in stress analysis, was measured by nanoindentation technique using a nanoindenter (Anton Paar, TTX NHT, Germany). For nanoindentation measurements, the coated samples were metallographically polished using 0.06 μm Al_2O_3 powder for 1 h followed by ultrasonic cleaning in acetone. A typical experiment of controlled loading and unloading by a Berkovich diamond nanoindenter (load range 0–80 mN) was performed on the coating surface. The conditions of the measurement are as follows: at a room temperature (25 °C) and at a relative humidity around 45%. The typical load/displacement curves were used to calculate the elastic modulus of the coatings.

The choice of a diffraction peak selected for residual stress measurement impacts significantly on the precision of the method. The higher the diffraction angle, the greater the precision. Then, several XRD measurements are taken at high 2theta peak position diffraction angle of 139.3° and diffraction plane (522) of the HAp at different psi tilts, and several values of $\varepsilon_{\psi\varphi}$ are determined. The stress tensor can be derived by three sets of measurements of strain at $\varphi = 0°$, 45°, 90°. The stress in coatings can then be calculated from a plot with basic knowledge of the elastic properties of the material. For each of the φ angles of 0°, 45° and 90°, 11 ψ (0, ± 18, ± 26, ± 33, ± 39, ± 45) tilts were examined to achieve data. The penetration depth into the sample surface should be sufficient for a stress tensor measurement. Therefore, the longer wavelength (less energetic) chromium Kα radiation was selected as x-ray tube, which penetrates further into the HAp coating than the more energetic copper Kα. The Kβ filter was also used to remove the contribution of the Kβ emission from the x-ray source. It is made from an element whose atomic

Table 2 The x-ray diffraction conditions by $\sin^2\psi$ method

Diffraction plane (h k l)	5 2 2
Equipment	Bruker D8 Advance
Diffraction angle, deg	139.3
Characteristic x-ray	Cr-Kα
Kβ filter	Vanadium
Tube voltage, kV	30
Tube current, mA	50

number (Z) is one less that the anode material, for a chromium anode x-ray tube the correct beta filter is vanadium (Table 2).

The three-point bending fatigue tests were carried out using a servo-electric testing machine (SEL-M010, Thelkin GmbH, Switzerland) to apply cyclic stresses at room temperature and frequency of 10 Hz. In this test, the flat specimen is placed on two parallel supports with the coating facing downward. The fatigue strength versus number of cycles to failure (S–N curves) of both coated Ti specimens were derived at a sinusoidal constant amplitude (R = 0).

## Results

Elastic Modulus of HAp Coatings

Indentation tests along with three-point bend tests were utilized for the determination of elastic modulus (E) of the HAp coatings. The load/displacement experiments were repeated on three independent locations of the surface of each coating specimen. The value of elastic modulus was extracted from the gradient of unloading curve using Oliver and Pharr's approach (Ref 17), S, according to the following equation:

$$S = \frac{dP}{dh} = \sqrt{\frac{4A}{\pi}} E_r \qquad \text{(Eq 4)}$$

$$\frac{1}{E_r} = \frac{(1 - v_s^2)}{E_r} + \frac{(1 - v_i^2)}{E_i} \qquad \text{(Eq 5)}$$

where P is the applied load, h is the indentation depth, A is the contact area, v is the Poisson's ratio and the subscripts r, s and i correspond to the reduced modulus of the system, the sample and the diamond indenter.

The load/displacement curves of indentations of the HAp coatings are shown in Fig. 4. The mean elastic modulus, assuming a Poisson's ratio of 0.28 (Ref 14) was measured to be 32.9 ± 3.5 GPa and 63.1 ± 2.9 GPa for HAp coating (APS) and HAp coating (VPS), respectively.
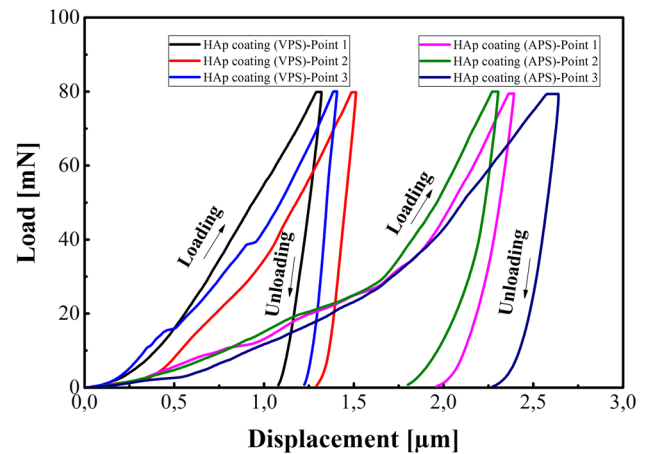
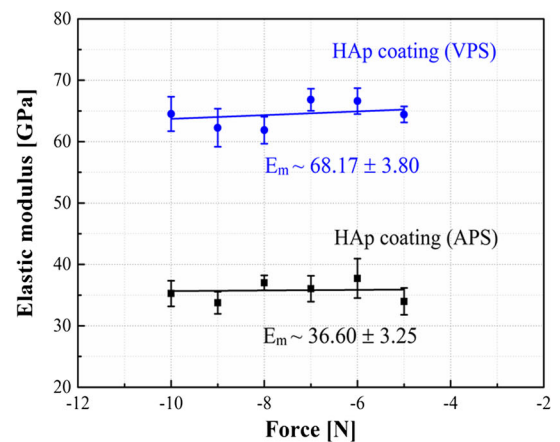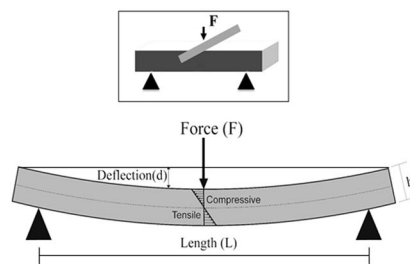**Fig. 4** Load/displacement curves of HAp coating (APS) and HAp coating (VPS)

Significantly higher levels of elastic modulus were observed for HAp coatings deposited in vacuum relative to HAp coating, when air plasma sprayed. The different elastic properties of two produced coatings can be attributed to their different microstructural characteristics. Elastic modulus of the plasma-sprayed coatings is highly influenced by the composition, microstructure as well as the crystallinity of the coatings. In the case of HAp ceramic coatings produced in atmosphere, heat is continuously lost by forced air convection and cold pockets are introduced into the spray stream due to turbulence of plasma jet. Micro-cracks can be generated at the interface or inner particle at the time of impact due to the lack of plasticity. The amorphous phases and oxide contamination can also form from the liquid in addition to hydroxyapatite if it is rapidly cooled. The porosity, micro-cracks and amorphous phases on the microstructure of HAp lead to a decrease in the elastic modulus of the bulk coating (Ref 18-20). In contrast to APS, the high velocity and the short dwell time of the particle in the plasma jet associated with VPS result in crystallized coating with high density (Ref 21). Some literature values of elastic modulus for HAp and the measurement methods are listed in Table 3. The elastic modulus of thermal sprayed HAp coatings was reported to be between 20 and 110 GPa (Ref 20, 22-24) which is much lower than that of the bulk sintered HAp material (Ref 25, 26), due to the crack network in the coatings. One-to-one comparison between the reported elastic modulus data and the data measured in this study cannot be yield directly, due to the various deposition method, microstructure and the measurement methods of the elastic modulus. Nevertheless, the present elastic modulus data are well in agreement with the reported data. The results imply a considerably improvement in low-pressure Hap-sprayed coatings. This arises from higher particle velocities and an absence of oxidation for VPS, which leads to the higher

Table 3 Elastic modulus of HAg coating from various studies

	HAp types	Elastic modulus, GPa	
		Method	Value, GPa
Bulk HAp			
Rao et al. (Ref 25)	Synthetic HAp compact	Ultrasonic interferometry	108
Van Dijk et al. (Ref 26)	Sintered at 1250 °C	Pulsed echo technique	117
HAp coating			
Yang et al. (Ref 20)	APS	Three-point bending	22.8
Gross et al. (Ref 22)	APS	Nanoindentation	48-110
Li et al. (Ref 23)	(HVOF) process	Three-point bending	24.8
Dey et al. (Ref 24)	MPS-HAP	Nanoindentation	$\sim$ 60–100
This study	APS	Nanoindentation/three-point bending	$\sim$ 33/$\sim$ 36.6
This study	VPS	Nanoindentation/three-point bending	$\sim$ 63/$\sim$ 68.2

APS, atmospheric plasma spraying; VPS, vacuum plasma spraying; HVOF, high-velocity oxy-fuel; MIPS, micro-plasma-sprayed coating

Fig. 5 Elastic modulus of HAp coatings determined by the three-point bending test

real contact area between lamellae of HAp coating. A peculiar feature known as pop-in was detected in the load/displacement curves of both HAp coatings. These pop-in behaviors may be induced by the presence of the defects or cracks in the coating (Ref 27).

Since the indentation test is primarily a local-phase-dependent method, measurements of elastic modulus of the entire HAp coatings were taken as well as using a standard three-point bending test and rule-of-mixture approximation. The value of elastic modulus was calculated from the relationship:

$$E = \frac{FL^3}{4bh^3\delta},$$ (Eq 6)

where E is the Young's modulus, F is the load, L is the span between supports, b is the specimen width, h is the specimen thickness and δ is the deflection at midspan. As shown in Fig. 5, the average values of elastic modulus of 36.6 GPa for HAp (APS) coating and 68.2 GPa for HAp

(VPS) coating were obtained, which are in the same range of values determined by indentation tests.

Residual Stress Tensor by $\sin^2\psi$ Method

Two types of coating specimens, i.e., atmospheric plasma-sprayed coating HAp (APS) and vacuum plasma-sprayed coating HAp (VPS) on titanium, were examined separately using the methodology outlined above. Plots of lattice strain $\varepsilon_{\psi\varphi}$ versus $\sin^2\psi$ are shown for the (522) reflection of the both coatings in Fig. 6(a) (APS coating) and Fig. 6(b) (VPS coating) at three rotation angles: (a) at $\varphi = 0°$, b) $\varphi = 45°$ and c) $\varphi = 90°$. The peak splitting is observed in the both samples while measuring $\pm\ \psi$ orientation. This is due to the existence of a non-equiaxial stress system, produced by shear stresses. Results were corrected for Lorentz polarization and absorption as well as a sloping background intensity. An algorithm is described for fitting Pearson VII distribution functions to determine the position of the $K_{\alpha1}$ component, eliminating errors
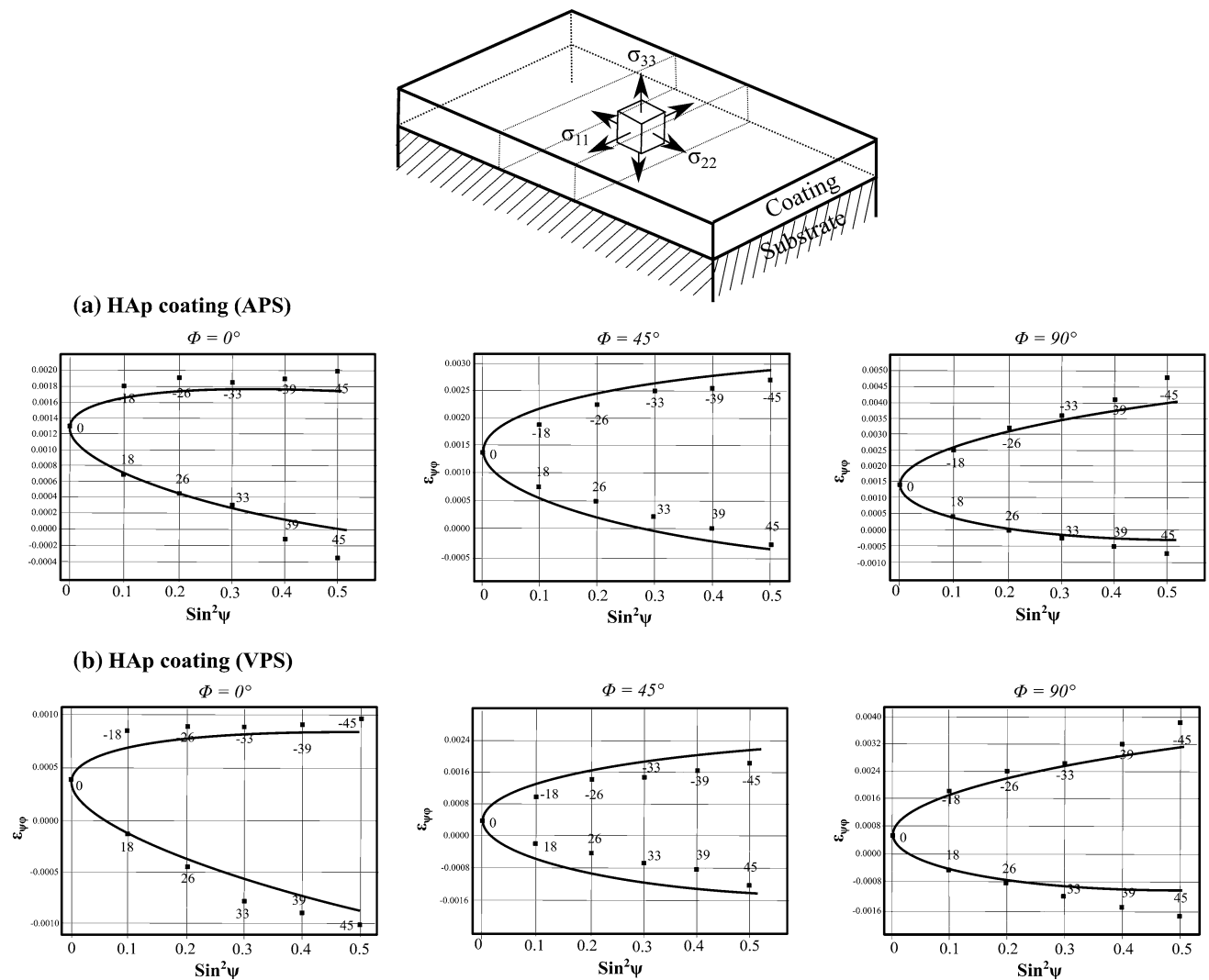
Fig. 6 Strain measurement of (a) HAp coating (APS, produced in atmosphere) and (b) HAp coating (VPS, produced in vacuum) in the middle of specimen at positive and negative values of the angle ψ

caused by defocusing of diffraction peaks of intermediate breadth. The method has been demonstrated to provide a more reliable method of determining lattice spacing in residual stress measurement than the other methods of fitting such as parabolic profiles by least squares regression for diffraction peaks of intermediate breadth (Ref 28).

The values of stress components for approximately 11 µm HAp coating deposited onto titanium can be obtained based on plots of $\varepsilon_{\psi\varphi}$ versus $\sin^2\psi$ and Eq 7. The average penetration depth z is calculated by:

$$z = \frac{\sin^2\theta - \sin^2\varphi}{2\mu\sin\theta\cos\varphi}, \qquad \text{(Eq 7)}$$

where μ is the linear absorption coefficient, θ is the Bragg angle of diffraction and ψ is defined in Fig. 1. In addition to the normal stress, shear stress exists in the direction of the surface normal, and then, the positive and negative ψ-inclination data split into two distinct branches as shown in Fig. 6(a) and (b). A significant splitting is observed in all $\varepsilon_{\psi\varphi}$ versus $\sin^2\psi$ plots. The stress tensors for two coatings are summarized in Table 4. These findings indicated that the surface of the HAp coatings showed an inhomogeneous stress distribution. One reason for this is the low thermal conductivity of the HAp material, which leads to a temperature gradient along the sphere particle during thermal spraying and formation of non-equilibrium phases during cooling. Since temperature during thermal spraying is often relatively high and stress levels can vary sharply with depth, the plastic flow occurs preferentially at certain levels within coating. When the molten particle impinges onto the surface, it deforms and begins to spread outward. The particles are then rapidly quenched due to heat transfer to the substrate resulting in tensile stress in the coating, commonly referred to as quenching stress. Furthermore, the

residual stress states in the thermal sprayed coatings caused also by the difference in the thermal expansion coefficient and the elastic modulus of the coating material and substrate material.

The residual stress of HAp coating has been measured in some investigations. Sergo et al. (Ref 29) determined the residual stress values in HAp coating on Ti6Al4 V to be tensile (100 MPa) when deposited in air and compressive (60 MPa) when deposited in a vacuum. They have also concluded that the tensile stresses enhance dissolution and compressive stresses impede dissolution of the coating. Furthermore, Yang et al. (Ref 14) measured also the biaxial stresses in the plasma-sprayed HAp coating in compressive states.

The stress calculation results in this study demonstrated the presence of triaxial stress in thermal sprayed HAp coatings. The comparison of two coating samples in this study indicated that the tensile normal stress distributions are present on both HAp coatings while the coating produced in air showed higher tensile stress values. The shear stress tensor component σ_{13} is compressive in both coatings, but it is higher for HAp coating produced in vacuum. The published data of residual stress for the HAp coating are given in Table 5. Compressive stress in the coating may be beneficial for its mechanical properties, since it would close the existing cracks and suppress crack propagation.

The origin and growth of cracks is provoked by shear stresses while the coated substrate is under external loading. Cracking of a coating is possible when tensile stresses develop. Figure 7 indicates distinctly micro-cracks distributed across the surface and cross section of HAp (APS) coating that were not interconnected and likely caused due to residual tensile stress, whereas the microstructure of HAp (VPS) coating (Fig. 8) is dense with very fine micro-cracks. HAp coating produced in vacuum exhibits a greater uniformity and a relatively high density compared with an air plasma-sprayed coating. Under tensile stress conditions, through-thickness cracks may develop from preexisting defects in the coating and these generate shear stress along the interface which may result in fracture.

Plasma spraying is a highly complex deposition process because of the interacting parameters particularly thermal exchanges between the plasma zone, powder particles and substrate. During plasma spraying process, powder particles were injected into the high-temperature plasma jet (about 10,000–20,000 °C) undergoing an extremely high heating rate. Within the plasma, the particles are then heated and accelerated toward the substrate surface where they deform into lamellae and subsequently solidify. Heat transfer from a particle to the surrounding plasma gas and the cooling rates during solidification plays an important role in determining the properties of the solidified deposit. Depending on the medium of plasma spraying process, accelerated particles strikes the substrate at a fully molten or partially molten state. Because of the low thermal conductivity of the ceramic HAp, the particles are rather slowly heated and thus impinge at the substrate in a partially molten form comprising of a liquid shell and a solid core at impact which affects the final characteristics of the coating and the internal stresses after deposition. The predominant factors are heat exchange of powder particles in the plasma jet and particle–substrate interactions within the plasma. Consequently, the different nature of the

Table 4 Residual stress tensors of HAp (APS) and HAp (VPS) coatings using $\sin^2\psi$ method

Specimen	Stress components σ_{ij}, MPa		
HAp (APS)	78.9 ± 24.4	16.3 ± 13.0	-15.4 ± 3.5
	16.3 ± 13.0	134.0 ± 24.4	45.6 ± 3.5
	-15.4 ± 3.5	45.6 ± 3.5	106.1 ± 11.7
HAp (VPS)	14.9 ± 28.2	12.0 ± 26.1	-31.9 ± 7.0
	12.0 ± 26.1	117.3 ± 18.2	31.8 ± 7.0
	-31.9 ± 7.0	31.8 ± 7.0	66.2 ± 22.7

Table 5 Residual stresses of HAp coating from various studies

|	HAp types	Residual stress, MPa	
		Method	Value, MPa
Sergo et al. (Ref 29)	APS	Raman piezo-spectroscopy	$+ 100$
Sergo et al. (Ref 29)	VPS	Raman piezo-spectroscopy	$- 80$
Yang et al. (Ref 14)	APS	XRD $\sin^2\psi$ method	$\sigma_1 = -5.2$
			$\sigma_2 = -2.5$
This study	APS	XRD $\sin^2\psi$ method	$\begin{pmatrix} 78.9 \pm 24.4 & 16.3 \pm 13.0 & -15.4 \pm 3.5 \\ 16.3 \pm 13.0 & 134.0 \pm 24.4 & 45.6 \pm 3.5 \\ -15.4 \pm 3.5 & 45.6 \pm 3.5 & 106.1 \pm 11.7 \end{pmatrix}$
This study	VPS	XRD $\sin^2\psi$ method	$\begin{pmatrix} 14.9 \pm 28.2 & 12.0 \pm 26.1 & -31.9 \pm 7.0 \\ 12.0 \pm 26.1 & 117.3 \pm 18.2 & 31.8 \pm 7.0 \\ -31.9 \pm 7.0 & 31.8 \pm 7.0 & 66.2 \pm 22.7 \end{pmatrix}$
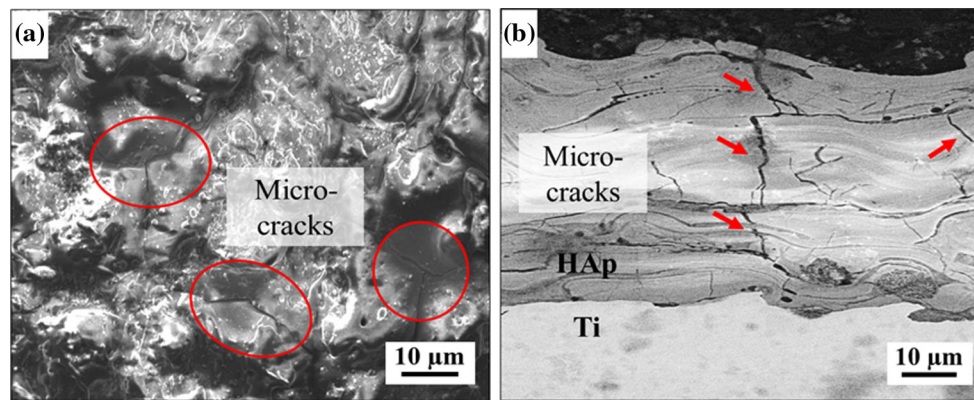
Fig. 7 SEM picture of HAp coating produced in atmosphere: (a) the surface, (b) the cross section
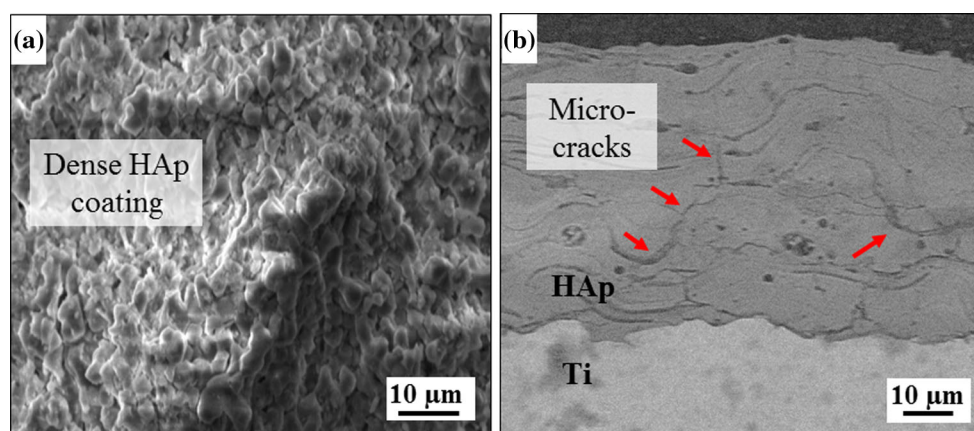

Fig. 8 SEM picture of HAp coating produced in vacuum: (a) the surface (b), the cross section

internal structure within lamellae produced by rapid solidification results in different material properties in two produced coatings. The cooling rate of the splats is mainly controlled by the quality of the contact with the substrate. The critical parameters comprise the particle velocity and temperature at impact, the oxidation of the particles, the temperature gradient within the particle and the substrate temperature. In the case of HAp ceramic coatings produced in atmosphere, heat is continuously lost by forced air convection during deposition and cooling down which lead to the large temperature gradients within ceramic powder particles. Due to lack of plasticity, micro-cracks can be generated at the time of impact between brittle ceramic portions of particles at the interface or inner particle. For VPS system, the coating deposition process takes place in a vacuum chamber which provides an inert atmosphere under low pressure (Ref 30). Consequently, the plasma jet velocity and particle impact velocity increase in vacuum, and particles deform them further and cover a greater surface area.

X-ray Analysis of HAp Coatings

X-ray diffraction data of the starting HAp powder and as-deposited coatings were acquired by x-ray diffractometer and using Cu-Kα radiation operated at 40 kV and 40 mA (Fig. 9). The main peaks of hydroxyapatite with high intensity still appeared in HAp coating deposited on Ti substrate, which meant that microstructures of the coating were mainly composed of HA phase. However, some phases of tricalcium phosphate (α-TCP and β-TCP) and calcium oxide (CaO) were also detected in HAp (APS) coating as shown in Fig. 9(b). The formation of these phases found in coatings can be easily explained by the thermal stability of apatite resulted from the rapid cooling rate of the spraying process. The decomposition of HAp cannot be avoided during plasma spraying process under such a high temperature.

During the plasma spraying process, the interaction of plasma plume with the ambient atmosphere affects the plasma/particle interaction and the microstructure of the
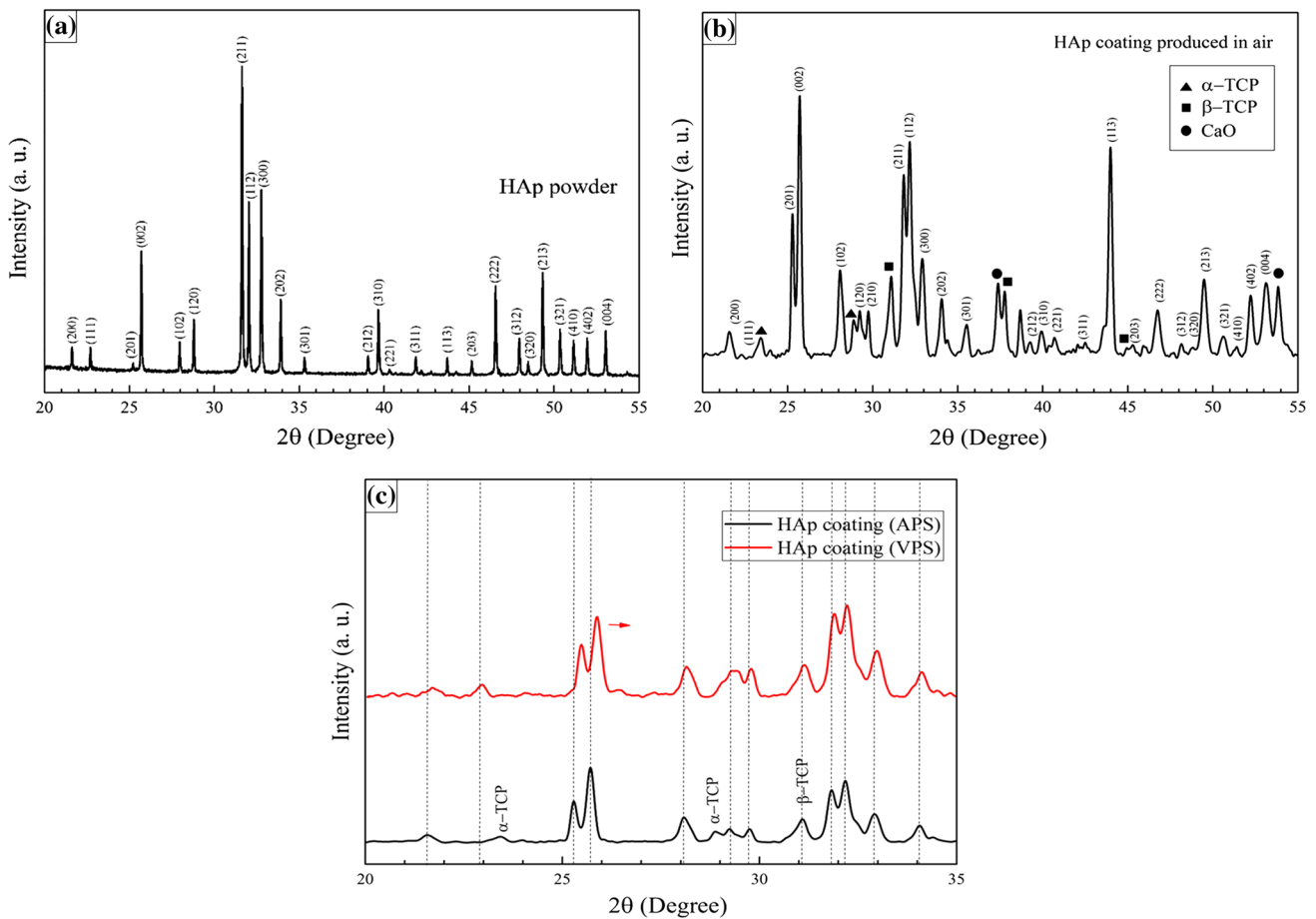
Fig. 9 XRD patterns of (a) raw HAp powder (b) HAp coating (APS). (c) A comparison of HAp (APS) and HAp (VPS) coatings

coating. The high-temperature droplets were propelled to and subsequently impacted on the substrate surface to form coating. The heat would be quickly absorbed and transferred through substrate, which resulted in rapid solidification of the molten HAp droplets and formation of amorphous phase on the substrate surface. As a result, the crystallinity of the HAp coating decreases during deposition process. Furthermore, the change in the phase composition and introduction of residual stresses take place in the HAp coatings due to the high temperature involved in the process. A remarkable shift of XRD pattern in HAp (VPS) is shown in Fig. 9(c), which meant that the lattice constants are different in HAp coating produced in vacuum compared with HAp coating produced in air. It can be related to the residual stresses within the coating which induce change in inter-planar spaces causing a shift in the diffraction pattern. By precise measurement of this shift, the change in the inter-planar spacing can be evaluated and thus the strain within the material deduced. Typically, only the shift in the peak position between different ψ-tilts is needed for accurate
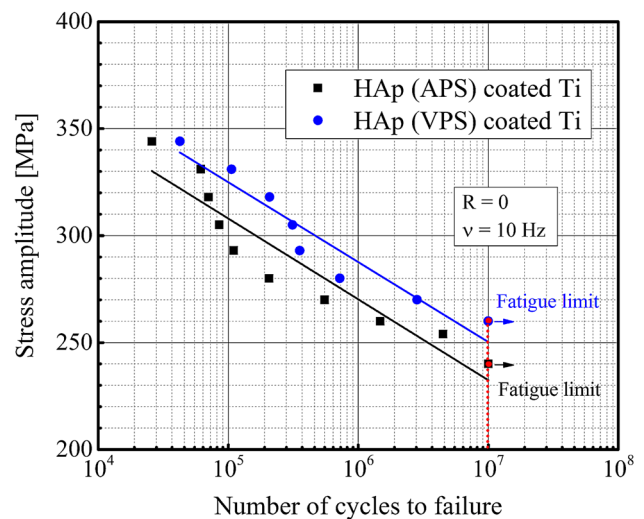

Fig. 10 S–N comparative curves of HAp (APS)- and (VPS)-coated Ti subjected to the bending loading

stress determination (Ref 16). The stress states can be expected to be more inhomogeneous due to the high local solidification stresses in the particles.
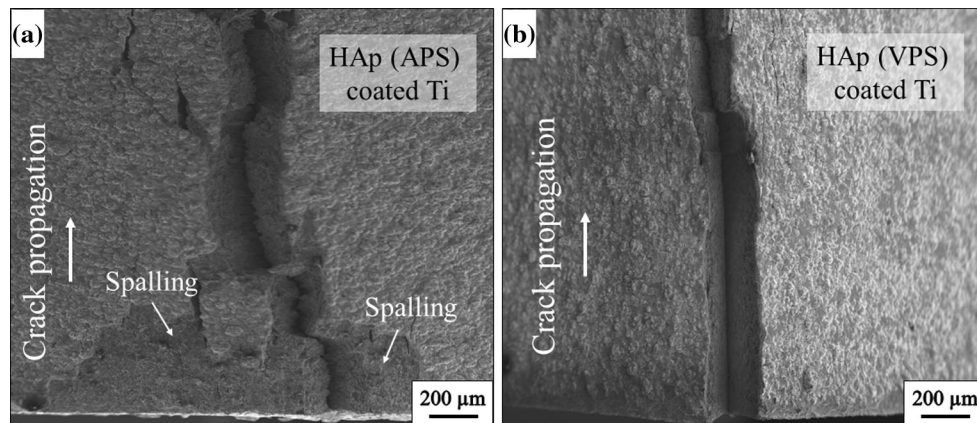
Fig. 11 SEM surface micrograph of (a) HAp (APS)-coated Ti (b) HAp (VPS)-coated Ti after fatigue failure

Fatigue Test Results

Experimental results from the fatigue bending test are shown in Fig. 10. Fatigue strength was considered as the complete fracture of specimen or 10^7 load cycles (fatigue limit). A significant decrease in fatigue life of the APS-coated Ti can be noted in comparison with VPS-coated Ti. Two red points are marked on the curves for the both coated specimens at 10^7 cycles. These two points were considered as the fatigue limit that were 240 MPa and 260 MPa for the APS- and VPS-coated Ti, respectively. The improvement in fatigue strength of VPS-coated specimens can be attributed to the lower tensile residual stresses presented in HAp coating. Furthermore, it is important to evaluate the coating adherence to the substrate after fatigue failure. SEM micrographs of two coated specimens failed at stress amplitude 280 MPa are shown in Fig. 11. A spalling of the HAp occurred in APS coating under cyclic loading (Fig. 11a), whereas the VPS coating remains completely adhered to the substrate even after cracking (Fig. 11b).

Conclusion

The strength and lifetime of the plasma-sprayed coatings are significantly influenced by the microstructure of the coating and residual stress field induced during coating deposition. In the plasma spraying process, the coating and the substrate materials undergo disparate thermal histories giving rise to thermal stresses, in that one is being cooled while the other is being heated (Ref 31). Since the thermal diffusivity increases with increasing contact temperature, preheating of the substrate leads to higher diffusive bonding and thus higher physical adhesion of the coating to the substrate. Oxygen-reactive substrate materials, such as Ti

and its alloys, can be preheated prior to spraying because of their thermal stability. The properly substrate preheating has significant influence on reduction in residual stress in HAp coating during plasma spraying process (Ref 32). Increasing the preheating temperature can obviously decrease the temperature difference between coating and substrate and, hence, the difference in coefficients of thermal conductivity of HAp and Ti. Furthermore, heating the substrate removes moisture and other volatile contaminants and slows the solidification rate of impinging particles allowing them to make better contact with the substrate and consequently better coating adhesion. Preheating produces an intermediate oxide sublayer on the surface which can change its thermal contact resistance and reduce the cracking of HAp coating.

The elastic modulus of HAp plasma-sprayed coatings produced in air (APS) and vacuum (VPS) has investigated by nanoindentation technique and three-point bending test. The VPS-deposited coating exhibited higher elastic modulus values than the APS-deposited coatings. This can be attributed to the presence of the pores, micro-cracks and amorphous phases in addition to hydroxyapatite inside the HAp coating deposited in atmosphere. Furthermore, increasing the impact velocity of particles in vacuum can generate high plastic deformed layer resulting in lower oxidation, lower porosity and denser coating, compared with atmospheric plasma spraying process. Residual stresses in thermally sprayed coatings can be considered as the sum of quenching stress arising from the contraction during rapid cooling of individual spray particles, tensile thermal stresses build up during the cooling process, as well as a compressive peening stress is due to impact of high-velocity spray particles. In the case of HAp plasma-sprayed coating, most of the stress comes from tensile stress originating from splat quenching and tensile thermal stress due to higher thermal coefficient of the HAp

$(\alpha_{HAp} = 11.5 \times 10^{-6} \text{ K}^{-1})$ compared with that of the Ti substrate $(\alpha_{Ti} = 8.9 \times 10^{-6} \text{ K}^{-1})$ (Ref 13). Therefore, the final stress state across the plasma-sprayed HAp coating is expected to be tensile. The components of the internal stresses in plasma-sprayed HAp coatings have measured by the $\sin^2\psi$ method. This method allows measurement of the local stresses down to the sub-micrometer scale within the coating. A splitting behavior in the $\varepsilon_{\phi\psi}$ versus $\sin^2\psi$ plots was observed due to the presence of shear stresses normal to the surface. The stress components values showed that the inhomogeneous normal stresses can be significant for both APS and VPS coatings, and these are tensile in nature for both HAp coatings. The fatigue results indicated an improvement in fatigue life in VPS-coated specimens compared with APS-coated specimens. The reason can be higher tensile stress values presented in coating produced in air which promotes multiple cracking of the coating deposited in air, whereas lower tensile stress values within HAp coating produced in vacuum may suppress the microcracks and can be beneficial for fatigue durability.

References

1. S.V. Dorozhkin and M. Epple, Biological and Medical Significance of Calcium Phosphates, *Angew. Chem. Int. Ed.*, 2002, **41**(17), p 3130-3146

2. L.T. de Jonge, S.C. Leeuwenburgh, J.G. Wolke, and J.A. Jansen, Organic–Inorganic Surface Modifications for Titanium Implant Surfaces, *Pharm. Res.*, 2008, **25**(10), p 2357-2369

3. H. Daugaard, B. Elmengaard, J.E. Bechtold, T. Jensen, and K. Soballe, The Effect on Bone Growth Enhancement of Implant Coatings with Hydroxyapatite and Collagen Deposited Electrochemically and by Plasma Spray, *J. Biomed. Mater. Res. Part A*, 2010, **92**(3), p 913-921

4. W.S.W. Harun, R.I.M. Asri, J. Alias, F.H. Zulkifli, K. Kadirgama, S.A.C. Ghani, and J.H.M. Shariffuddin, A Comprehensive Review of Hydroxyapatite-Based Coatings Adhesion on Metallic Biomaterials, *Ceram. Int.*, 2017, **44**(2), p 1250-1268

5. J. R. Davis, Ed., Introduction to Thermal Spray Processing, *Handbook of Thermal Spray Technology*, p 3–13

6. T.W. Clyne and S.C. Gill, Residual Stresses in Thermal Spray Coatings and Their Effect on Interfacial Adhesion: A Review of Recent Work, *J. Therm. Spray Technol.*, 1996, **5**(4), p 401

7. Y.C. Yang and E. Chang, Influence of Residual Stress on Bonding Strength and Fracture of Plasma-Sprayed Hydroxyapatite Coatings on Ti–6Al–4V Substrate, *Biomaterials*, 2001, **22**(13), p 1827-1836

8. Z. Gan, H.W. Ng, and A. Devasenapathi, Deposition-Induced Residual Stresses in Plasma-Sprayed Coatings, *Surf. Coat. Technol.*, 2004, **187**(2–3), p 307-319

9. A.G.E.A. Rabiei and A.G. Evans, Failure Mechanisms Associated with the Thermally Grown Oxide in Plasma-Sprayed Thermal Barrier Coatings, *Acta Mater.*, 2000, **48**(15), p 3963-3976

10. Y. Otsuka, H. Kawaguchi, and Y. Mutoh, Cyclic Delamination Behavior of Plasma-Sprayed Hydroxyapatite Coating on Ti–6Al–4V Substrates in Simulated Body Fluid, *Mater. Sci. Eng. C*, 2016, **67**, p 533-541

11. P. Millet, E. Girardin, C. Braham, and A. Lodini, Stress Influence on Interface in Plasma-Sprayed Hydroxyapatite Coatings on Titanium Alloy, *J. Biomed. Mater. Res.*, 2002, **60**(4), p 679-684

12. Y.C. Yang and E. Chang, Measurements of Residual Stresses in Plasma-Sprayed Hydroxyapatite Coatings on Titanium Alloy, *Surf. Coat. Technol.*, 2005, **190**(1), p 122-131

13. A. Dey and A.K. Mukhopadhyay, Evaluation of Residual Stress in Microplasma Sprayed Hydroxyapatite Coating by Nanoindentation, *Ceram. Int.*, 2014, **40**(1), p 1263-1272

14. Y.C. Yang, E. Chang, B.H. Hwang, and S.Y. Lee, Biaxial Residual Stress States of Plasma-Sprayed Hydroxyapatite Coatings on Titanium Alloy Substrate, *Biomaterials*, 2000, **21**(13), p 1327-1337

15. R.B. Heimann, Tracking the Thermal Decomposition of Plasma-Sprayed Hydroxylapatite, *Am. Miner.*, 2015, **100**(11–12), p 2419-2425

16. M.E. Fitzpatrick, A.T. Fry, P. Holdway, F.A. Kandil, J. Shackleton, and L. Suominen, *Determination of Residual Stresses by X-ray Diffraction, Issue 2, Measurement Good Practice Guide No. 52*, National Physical Lab, 2005, p 5–44

17. W.C. Oliver and G.M. Pharr, An Improved Technique for Determining Hardness and Elastic Modulus Using Load and Displacement Sensing Indentation Experiments, *J. Mater. Res.*, 1992, **7**(6), p 1564-1583

18. Y.C. Tsui, C. Doyle, and T.W. Clyne, Plasma Sprayed Hydroxyapatite Coatings on Titanium Substrates Part 1: Mechanical Properties and Residual Stress Levels, *Biomaterials*, 1998, **19**(22), p 2015-2029

19. A. Dey and A.K. Mukhopadhyay, Suppl 1-M5: Nanoindentation Study of Phase-pure Highly Crystalline Hydroxyapatite Coatings Deposited by Microplasma Spraying, *Open Biomed. Eng. J.*, 2015, **9**, p 65

20. Y.C. Yang and C.Y. Yang, Mechanical and Histological Evaluation of a Plasma Sprayed Hydroxyapatite Coating on a Titanium Bond Coat, *Ceram. Int.*, 2013, **39**(6), p 6509-6516

21. J.R. Davis, Ed., *Handbook of Thermal Spray Technology*, ASM International, Russell Township, 2004

22. S. Saber-Samandari and K.A. Gross, Nanoindentation Reveals Mechanical Properties Within Thermally Sprayed Hydroxyapatite Coatings, *Surf. Coat. Technol.*, 2009, **203**(12), p 1660-1664

23. H. Li, K.A. Khor, and P. Cheang, Properties of Heat-Treated Calcium Phosphate Coatings Deposited by High-Velocity Oxy-Fuel (HVOF) Spray, *Biomaterials*, 2002, **23**(10), p 2105-2112

24. A. Dey, A.K. Mukhopadhyay, S. Gangadharan, M.K. Sinha, D. Basu, and N.R. Bandyopadhyay, Nanoindentation Study of Microplasma Sprayed Hydroxyapatite Coating, *Ceram. Int.*, 2009, **35**(6), p 2295-2304

25. H. Rao, W.A. Thompson, J.L. Katz, and R.A. Harper, Elastic Constants of the Composite System Hydroxyapatite-Dicalcium Phosphatedihydrate, *J. Dent. Res.*, 1976, **55**, p 708

26. H.J.A. Van Dijk, N. Hattu, and K. Prijs, Preparation, Microstructure and Mechanical Properties of Dense Polycrystalline Hydroxy Apatite, *J. Mater. Sci.*, 1981, **16**(6), p 1592-1598

27. A. Dey and A.K. Mukhopadhyay, *Nanoindentation of Brittle Solids*, CRC Press, Cambridge, 2014, p 350-353

28. P.S. Prevéy, The Use of Pearson VII, Distribution Functions in X-Ray Diffraction Residual Stress Measurement, *Adv. X-Ray Anal.*, 1986, **29**, p 103-111

29. V. Sergo, O. Sbaizero, and D.R. Clarke, Mechanical and Chemical Consequences of the Residual Stresses in Plasma Sprayed Hydroxyapatite Coatings, *Biomaterials*, 1997, **18**(6), p 477-482

30. H. Singh, B.S. Sidhu, D. Puri, and S. Prakash, Use of Plasma Spray Technology for Deposition of High Temperature Oxidation/Corrosion Resistant Coatings–A Review, *Mater. Corros.*, 2007, **58**(2), p 92-102

31. H.W.W. Wong, Heat Transfer Analysis of the Plasma Spray Deposition Process, Ph.D. Thesis, University of British Columbia, 1997

32. B.R. Gligorijević, M. Vilotijević, M. Šćepanović, N.S. Vuković, and N.A. Radović, Substrate Preheating and Structural Properties of Power Plasma Sprayed Hydroxyapatite Coatings, *Ceram. Int.*, 2016, **42**(1), p 411-420